Lu, Q., Scarpa, F., Liu, L., Leng, J., & Liu, Y. (2018). An E-shape broadband piezoelectric energy harvester induced by magnets. *Journal of Intelligent Material Systems and Structures*, *29*(11), 2477-2491. https://doi.org/10.1177/1045389X18770871

An E-shape Broadband Piezoelectric Energy Harvester Induced by Magnets

Qingqing Lu[a,c], Fabrizio Scarpa[b], Liwu Liu[a], Jinsong Leng[c] and Yanju Liu[a,*]

[a] Department of Aerospace Science and Mechanics, No. 92 West Dazhi Street, Harbin Institute of Technology (HIT), P.O. Box 301, Harbin 150080, PR China
[b] Bristol Composites Institute (ACCIS), University of Bristol, Bristol, BS8 1TR, UK
[c] Center for Composite Materials and Structures, No. 2 Yikuang Street, Science Park of Harbin Institute of Technology (HIT), P.O. Box 301, Harbin, PR China

[*] Corresponding author.

Tel./FAX: +86-451-86414825.

E-mail addresses: yj_liu@hit.edu.cn

Abstract

We describe in this work a broadband magnetic E-shape Piezoelectric Energy Harvester (PEH) with wide frequency bandwidth. We develop first a nonlinear electromechanical model of the harvester based on the Hamilton variation principle that simulates the effect of the nonlinear magnetic restoring force at different spacing distances. The model is used to identify the distances existing between two different magnets that enable the system to perform with a specific nonlinearity. The performance of the E-shape PEH is also investigated thorough experiments, with E-shape energy harvesters at different spacing distances tested under several base accelerations excitations. We observe that the frequency domain output voltage of the system shows a general excellent controllable performance, with a widening of the frequency bandwidth. The half-power bandwidth of the linear energy harvester for a distance of 25mm is 0.8Hz only, which can be expanded to 2.67 Hz for the larger distance of 11mm between magnets. The energy harvester presented in this work shows promising performances for broad spectrum vibration excitations compared to conventional cantilever PEH systems with tip mass.

Keywords: Energy harvesting; Piezoelectric; Actuator

1. Introduction

Energy harvesting allows the capture of small amounts of energy from one or more surrounding energy sources. The energy is then converted into electricity, and then stored for later use. Examples of the application of energy harvesters range from lightweight systems to wireless sensor networks (Kim et al., 2011). Vibration energy harvesters are in general considered as eco-friendly designs, with long operational life and low maintenance costs compared to traditional batteries. Many research groups have devoted significant efforts to improve the performance of vibration energy harvesting systems. Piezoelectric energy harvesters have a special appeal, because piezoelectric materials possess high energy conversion rates from mechanical vibration to electrical power by using simple baseline designs.

Williams and Yates (1996) introduced the concept of vibration energy harvester for the first time in 1996. Since their seminal work, three main classes of energy harvesters have been designed to transfer vibrational energy into electrical power: the electrostatic (Mitcheson et al., 2004), electromagnetic (Arnold, 2007) and piezoelectric ones (Anton and Sodano, 2007; Priya, 2007). Piezoelectric energy harvesting has been particularly successful in vibration-based energy transduction applications, because of its relatively simple design and high energy transfer efficiency. Xu et al. (2013) have evaluated the key parameters that define the energy harvesting performance (including the generated electrical energy/power), and the mechanical to electrical energy conversion efficiency of a new ‘33’ mode PZT-Stack energy harvester. Ren et al. (2006) have investigated the energy harvesting

performance in 1-3 composites PMN-PT single crystals embedded in a soft epoxy matrix. Traditional PEHs typically consist in a cantilever beam with piezoelectric layers, a tip mass and an electrical circuit (Sodano et al., 2005). In order to obtain the maximum electrical power, traditional vibration-based energy harvesters have to be designed to match one or more of their natural frequencies to the base excitation frequencies (Erturk and Inman, 2008; Song et al., 2010; Rafique and Bonello, 2010; Lu et al., 2016). To overcome these technical limitations, some researchers have focused on increasing the bandwidth of PEHs. Some possible solutions for this problem involve the use of periodic tuning of the harvester resonance to match the excitation frequency in all the operative conditions. The baseline designs to improve the PEHs performance mainly consist in linear and nonlinear energy harvesters (Twiefel and Westermann, 2013). Shahruz (2006) has presented a theoretical study related to a linear piezoelectric generator array consisting in an ensemble of cantilevers with tip masses. The beams were modeled as SDOF systems. The tunability of the PEH bandwidth was provided by the appropriate design of the dimensions of the beams and the proof masses. Xue et al. (2008) introduced a novel design for a broadband PEH by integrating multiple linear piezoelectric bimorphs with different physical dimensions. Numerical calculations have shown that the operational frequency of the energy harvesters of this concept could be widened and shifted to the dominant excitation frequency band to achieve higher energy harvesting efficiencies. Qi et al. (2010) have also designed a novel nonlinear device using a clamped-clamped beam piezoelectric fiber composite generator. This particular PEH

design showed a wide-band energy harvesting performance compared to a traditional piezoelectric harvester with a single cantilever.

Another harvester configuration able to generate large bandwidths makes use of nonlinear bistable structures. The Reader is referred in this case to the energy harvesters made by bistable piezoelectric composite plates (Betts et al., 2012; Arrieta et al., 2013). Several other works (Harne and Wang, 2013; Wu et al., 2014; Harne et al., 2013) have focused on the dynamics of coupled linear oscillator-bistable energy harvester systems. Their results justify the holistic design approach used in linear-bistable coupled systems to enhance the performance and robustness of general bistable energy harvesters. Erturk et al. (2009, 2011) have presented a nonlinear broadband piezoelectric power generator induced by magnets. The magnetic PEH was a significant improvement compared to a traditional Duffing oscillator configuration. The experimental electromechanical trajectories of the magnetic PEH were instrumental to verify that the piezomagnetoelastic configuration proposed was feasible, and it could generate power an order of magnitude larger than the one provided by traditional piezoelastic counterparts at several frequencies. Masana and Daqaq (2011), and Daqaq et al. (2014) introduced other models and analysis of nonlinear structures for piezoelectric energy harvesters. Westermann et al. (2012) developed a mechanical model that describes a vibration-based piezomagnetoelastic energy harvester containing a piezoelectric cantilever beam and two permanent magnets. The same type of nonlinear PEH was also introduced by Ferrari et al. (2010, 2011); the experimental results of this single-magnet piezoelectric device showed a

400% improvement of the voltage generated by the converter, compared to the linear case. Su et al. (2014) presented a broadband magnet-induced dual-cantilever PEH. The new design featured a significant improvement in terms of operational bandwidth, compared to a traditional piezoelectric energy harvester. Kim and Seok (2014) looked at the dynamic modeling and bifurcation analysis of a bistable energy harvester, and the numerical results demonstrated the potential significant performance of this type of PEH design. Zhou et al. (2014) evaluated through theory and experiments the performance of a broadband piezoelectric based vibration energy harvester with a triple-well potential induced by the presence of a magnetic field. The performance of the PEH was improved by the use of tunable magnetic fields, and the frequency bandwidth could be also significantly expanded (Ramlan et al., 2009; Mann and Sims, 2009; Ramezanpour et al., 2016; Abdelkefi et al., 2016).

The aforementioned previous work mainly described an energy harvester constituted by a piezoelectric cantilever beam with a permanent magnet attached to the free end, while another stationary magnet was poled along the opposite direction and fixed to a reference heavy frame near the magnet. The design however is not compact, and it is also quite difficult to scale. In this paper we propose instead a novel bistable structure that consists of three piezoelectric cantilever beams, with three couples of magnets fixed at the end of each beam. We will demonstrate that with this design it is possible to obtain a more compact and scalable broadband PEH. The system shows nonlinear dynamic characteristics under the presence of a magnetic field; when the vibration-induced acceleration levels allow to overcome the potential

energy wells, the beam transits across different stable equilibrium positions. In this way, the piezoelectric materials can acquire larger strains and therefore - in theory - large voltages. Moreover, the frequency-response curves will tend to move towards the right (i.e., higher frequencies); this behavior leads to a broadening of the response bandwidth of these energy harvesters.

2. Design of the E-shape energy harvester

The nonlinear PEH system of this study is shown in Figure 1. The energy harvesting system is made from three cantilever beams and three groups of magnets. We use a $[0/90]_3$ carbon fiber laminate (T300/6509, Guangwei Composites Co. Ltd) to fabricate the three cantilever beams, because this cross-ply stacking sequence has a relatively low modal damping ratio associated to the first mode than other laminates (Paknejad et al., 2016). During the fabrication of the carbon fiber laminate the distributed PZT layers are bonded to the surface, which also act as electrodes here. The PZTs (PZT 5H, Sinoceramics Inc., China) are distributed as arrays on the two surfaces of the beam before the cure in autoclave. The curing temperature is 150 °C and the process lasts 2 hours. The direction of the polarization of the top and bottom PZT layers is the same, therefore the connection is a parallel one. Three groups of NdFeB magnets (Yongbang Magnets Co. Ltd) are fixed at the free end of each beam. The moment of the magnetic dipoles between two groups of magnets is $0.019 Am^2$. Both the model and the manufactured sample consist in three beams fixed along the same horizontal plane. In that sense, only the effect of the horizontal distance 'd' is here considered; the vertical displacement of the magnets along the z-direction will

however affect the magnetic force, and this point needs to be taken into account for a more refined analysis.

The E-shape energy harvester designed here features some particular characteristics compared to other piezoelectric energy harvesters. First of all, the system contains three cantilever beams, and that implies that more PZT layers can be connected to acquire electrical power. Secondly, the most notable difference between the proposed energy harvester and other ones described in open literature is that the traditional tip mass is replaced by magnets; the latter could be used both to adjust the natural frequency and to provide additional dynamic restoring forces during vibration. This is a departure from the majority of prototypes of piezoelectric cantilever beam energy harvesters, which use the tip mass just to adjust the resonance frequency, or use permanent magnets located near the free end of a ferromagnetic cantilever beam that need a complex and bulky frame as a fixture (Erturk et al., 2009). On the contrary, the E-shape energy harvester does not need an additional frame to fix the magnets, and the system is therefore simpler and more compact. The third feature of the E-shape design is its scalability: it is relatively easy to add an additional cantilever beam if one needs more power output.

3. Modeling of the E-shape energy harvester

The piezoelectric material used in this study is a PZT-5H layer attached to the surface of the cantilever beams, so the piezo-layer can be considered as a bending element. The PZT layer is poled along the z-axis, and the dynamic excitation is assumed to exist only along the z-axis; the piezoelectric material is therefore assumed

to experience only one-dimensional stresses along the x-direction. The constitutive equations for a linear piezoelectric material in a reduced matrix form can be expressed as follows:

$$\begin{aligned} T_1 &= c_{11}^E S_1 - e_{31} E_3 \\ D_3 &= e_{31} S_1 + \varepsilon_3^T E_3 \end{aligned} \tag{1}$$

In (1) S_1 is the strain component, T_1 is the stress, D_3 is the electric displacement, E_3 is the electric component, e_{31} is the piezoelectric constant and ε_3^T is the permittivity at constant strain. Furthermore, the 1 and 3 directions are here coincident with the x and z directions of Figure 1. The PZT layer is poled along the thickness direction (z-axis).

The governing equations of motion of the PEH can be derived following the Hamilton variational principle:

$$\int_{t_1}^{t_2} (\delta T - \delta U + \delta W) dt = 0 \tag{2}$$

The kinetic energy of the system can be written as:

$$T_i = \frac{1}{2}[\int_{V_s} \rho_s \dot{z}_i^{\,2} dV_s + \int_{V_p} \rho_p \dot{z}_i^{\,2} dV_p + M_{ti} \dot{z}_i^2 \big|_{x=L_m}], \quad i = 1,2,3 \tag{3}$$

Where V_s is the volume of the beam substructure and V_p is volume of the PZT layer. The densities ρ_s and ρ_p are referred to the beam and the PZT layer. The mass of the magnet is M_t, and L_m is the distance from the center of the magnet to the base. The transverse displacement along the z-direction at a distance x is indicated as z.

The total potential energy due to the mechanical strain energy and the

electrical energy can be expressed as (Song et al., 2010):

$$U_i = \frac{1}{2}\int_{V_s} \sigma_{s_i}\varepsilon_{si} dV_s + \frac{1}{2}\int_{V_p} \sigma_{pi}\varepsilon_{pi}\, dV_p - \frac{1}{2}\int_{V_p} E_p D_p\, dV_p\,, \quad i = 1,2,3 \quad (4)$$

Using the linear constitutive equation (1), we can further relate stress and electric displacement to strain according to:

$$\sigma_p = C_p\varepsilon_p - e_{31}E_p, \quad D_p = e_{31}E_p + \varepsilon_3 E_p \quad (5)$$

The electric field E_p can be related to the voltage by the relation $E_p = V(t)/t_p$. The stress in the substructure is expressed by Hooke's law as:

$$\sigma_s = C_s\varepsilon_s \quad (6)$$

The work done by the external force can be written as (Song et al., 2010):

$$W_i = -\int_{V_s} F(t) z dV_s - \int_A qV(t) dA - \int_0^L c\dot{z} dx + F_{mi} z\Big|_{x=L_m}\,, \quad i = 1,2,3 \quad (7)$$

In (7) q is the charge density and $V(t)$ is the electrical voltage. The magnetic force F_m can be derived using a dipole-dipole model (Figure 2).

The force within the magnetic dipole is given by (Tang and Yang, 2012):

$$F_{d-d} = \frac{3\mu_0 m_A m_B}{2\pi D^4} \quad (8)$$

where m_A, m_B are the moments of the magnetic dipoles, and μ_0 is the vacuum permeability. The expression of the magnetic force used here is different with the one described in the models shown in (Erturk et al., 2009, 2011; Daqaq et al., 2014; Westermann et al., 2012; Ferrari et al., 2010; Stanton et al., 2010); the specific model used in this study does not include the effect generated by the rotation of the magnets during the beam deflection. Here, we use three couples of repulsive magnets so the relation $m_A = m_B$ is valid.

The magnetic force around the z-direction can be written as:

$$F_{m1} = F_{mA-B} \bullet \sin\theta = \frac{3\mu_0 m_A m_B}{2\pi(\sqrt{d^2 + (z_1 - z_2)^2})^4} \bullet \frac{z_1 - z_2}{\sqrt{d^2 + (z_1 - z_2)^2}} \tag{9}$$

$$F_{m2} = F_{mC-B} \bullet \sin\theta = \frac{3\mu_0 m_C m_B}{2\pi(\sqrt{d^2 + (z_3 - z_2)^2})^4} \bullet \frac{z_3 - z_2}{\sqrt{d^2 + (z_3 - z_2)^2}} \tag{10}$$

The vertical magnetic force shown here can be expanded into its Taylor series around $|z_1 - z_2| = 0, |z_3 - z_2| = 0$. Here, z_1, z_2, z_3 are the transverse displacements of the magnet. The magnetic moments of beam-1, beam-2 and beam-3 are indicated as m_A, m_B, m_C. The spacing distance between two beams (beam-1 and beam-2, or beam-2 and beam-3) is d . We obtain the following expressions:

$$F_{m1} = \frac{3\mu_0 m_A m_B}{2\pi} \bullet \left(\frac{1}{d^5}(z_1 - z_2) - \frac{5}{6d^7}(z_1 - z_2)^3 + O((z_1 - z_2)^5) \right) \tag{11}$$

$$F_{m2} = \frac{3\mu_0 m_C m_B}{2\pi} \bullet \left(\frac{1}{d^5}(z_3 - z_2) - \frac{5}{6d^7}(z_3 - z_2)^3 + O((z_3 - z_2)^5) \right) \tag{12}$$

The resultant magnetic force acting on the middle cantilever beam around the z-direction is $-(F_{m1} + F_{m2})$. Here, we consider the positive force of the magnets acting along the z-direction. By using a modal decomposition method, the displacement function can be written as:

$$z(x,t) = \sum_{i=1}^{n} \phi_i(x) r_i(t) \tag{13}$$

Where $\phi_i(x)$ is the assumed mode shapes, $r_i(t)$ is the time-dependent generalized mechanical coordinate and *n* is the number of modes. The first mode shape of the cantilever beam can be expressed as (Erturk et al., 2009; Laura P A A et al., 1974; Kim et al., 2010):

$$\phi(x) = C_1(\cosh\beta x - \cos\beta x - A(\sinh\beta x - \sin\beta x)) \tag{14}$$

where $A = \left(\frac{\sin\beta L - \sinh\beta L + \beta\frac{M_t}{m}(\cos\beta L - \cosh\beta L)}{\cos\beta L + \cosh\beta L - \beta\frac{M_t}{m}(\sin\beta L - \sinh\beta L)} \right)$, and the constant C_1 can be evaluated by applying the orthogonality conditions. Substituting Eq. (14) into (13) and Eq. (12), (11), (7), (4), (3) into (2), the governing equations of this nonlinear energy harvester are:

$$\begin{cases} M_1\ddot{r}_1 + C_1\dot{r}_1 + K_1 r_1 - F_{m1} + \Theta V_1 = F_1(t) \\ -\Theta\dot{r}_1 + C_P\dot{V}_1 + \dfrac{V_1}{R} = 0 \\ M_2\ddot{r}_2 + C_2\dot{r}_2 + K_2 r_2 + (F_{m1} + F_{m2}) + \Theta V_2 = F_2(t) \\ -\Theta\dot{r}_2 + C_P\dot{V}_2 + \dfrac{V_2}{R} = 0 \\ M_3\ddot{r}_3 + C_3\dot{r}_3 + K_3 r_3 - F_{m2} + \Theta V_3 = F_3(t) \\ -\Theta\dot{r}_3 + C_P\dot{V}_3 + \dfrac{V_3}{R} = 0 \end{cases} \tag{15}$$

Where:

$$M_i = \int_0^L \rho_s h_s b_s \phi^2(x)ds + \int_{L_{p1}}^{L_{p2}} \rho_p h_p b_p \phi^2(x)ds + M_t\phi^2(x)\Big|_{x=L_m}$$

$$K_i = \int_0^L E_i \frac{b_s h_s^3}{12}\phi''^2(x)dx + \int_{L_{p1}}^{L_{p2}} c_{11}^E\left(\frac{b_p h_s^2 h_p}{2} + b_p h_s h_p^2 + \frac{2b_p h_p^3}{3}\right)\phi''^2(x)dx$$

$$\Theta = -\int_{L_{p1}}^{L_{p2}} \frac{e_{31} b_p (h_p + h_s)}{2}\phi''^2(x)dx$$

$$C_p = \frac{\varepsilon_{33}^s b_p (L_{p2} - L_{p1})}{2h_p}$$

$$F_i(t) = \Gamma_B A_0 \sin\omega t = \left[\int_0^L \rho_s h_s b_s \phi^2(x)ds + \int_{L_{p1}}^{L_{p2}} \rho_p h_p b_p \phi^2(x)ds + M_t\phi^2(x)\Big|_{x=L_m}\right] A_0 \sin\omega t$$

M_i, K_i, Θ and C_p are respectively the effective mass, stiffness, electromechanical coupling terms and capacitance. The parameters ρ_s, h_s, b_s, L represent the density, thickness, width and length of the substructure; ρ_p, h_p, b_p are

the density, thickness and width of the PZT layer, and L_{p1}, L_{p2} are the distances between the starting and ending positions of the PZT layer on the beams. We only consider a resistive load in this work. If the PEH system is connected to other electrical loads (such as a capacitance or a SSHI circuit), the model can be derived based on the formulation presented by Roundy et al. (2004), who described the modeling of different types of electrical loads.

In the model used in this paper we assume that the three couples of magnets vibrate only around the vertical direction. Each beam has two permanent magnets that attract each other, and are fixed at the free end. When the three groups of magnets are disposed like in Figure 2 the system will feature two stable conditions. Two groups of magnets are attached to the two outer beams on the free end of the structure, and the third group of opposed poled magnets is fastened to the free end of the inner beam. The magnetic force can be tuned by adjusting the distance between two beams. With the decrease of the distance between each beam, the magnetic force exerted on each cantilever beam will become larger. By combining Eqs. (11) and (12) we can simulate the magnetic force along the z-direction at different spacing distances. When the distance between two couples of magnets becomes narrow the restoring force around the z-direction increases, and assumes a nonlinear behavior ($\lambda = d / L$, d=17, 14, 11 *mm* - Figure 3). Conversely, when the distance between two magnets becomes large the system tends to become linear. As the spacing distance decreases to $\lambda = 0.2125$, the system will start to feature some nonlinearity. With spacing distances decreasing to $\lambda = 0.175$ and $\lambda = 0.1375$ the system shows a distinct symmetric double well

with two stable positions and one unstable equilibrium point at the origin. The bistable system will jump between two potential wells if the excitation can overcome the potential energy barriers. In the current design the bistability (stable states 1 and 2) is obtained by using the three groups of magnets (Figure 4). The system will therefore vibrate across different stable equilibrium positions when the excitation is sufficiently high to overcome the potential energy well.

4. Numerical simulations

To simulate the parametric features of the dynamic response and voltage output of the E-shape energy harvesting system we operate a dimensionless transformation of the governing equations by defining $r' = r_i / L$, $u = V_i / V_c$, $f = \left|\Gamma_B A_0 / KL\right|$, $\lambda = d / L$ and $V_c = -L\Theta / C_p$, $\zeta = C / 2M\omega_n$, $\omega_n = \sqrt{K / M}$. The quantity ω_n is the natural frequency for the linear case. The dimensionless frequency is defined as $\Omega = \omega_e / \omega_r$, where ω_r is the resonance frequency of the harvester coupled with the magnetic force under lower-level excitation. This resonance will shift towards lower frequencies when the repulsive magnetic spacing distance decreases (Tang et al., 2012). The simulations are aimed at identifying the behavior between u and Ω. The specific dimensions, mass, mechanical and piezoelectric properties used for the E-shape energy harvester system are shown in Table 1. The damping ratio is obtained from the average of three experimental FRFs (Frequency Response Functions) in the linear regime. An example of an experimental FRF is shown in Figure 5. The damping ratio is estimated as $\zeta = \dfrac{f_{upper} - f_{lower}}{2 f_r}$, where f_{upper}

and f_{lower} are two points that correspond to the half power bandwidth, and f_r is the natural frequency. The average damping ratio calculated at the end of the experiments is $\zeta = 0.015$. During the simulations, the initial boundary conditions and physical parameters are assumed to be the same, therefore the output voltage of the three simulated beams is also equal.

The numerical solution is performed using a Matlab Ode45 routine with the dimensionless independent variable Ω increased from 0.5 to 1.5 at constant intervals of 1/240. After the dimensionless transformation the spacing distance *d*=25, 17, 14, 11mm becomes $\lambda = 0.3125, 0.2125, 0.175, 0.1375$. Once the program completes one cycle the output data is taken as the initial value for the next step.

Figure 6 shows the results of the E-shape energy harvester under four different excitation accelerations ($\lambda = 0.2125$). When the base excitation is 0.5g, the response shows a slight stiffening towards high frequencies. After the excitation acceleration is increased the nonlinear behavior is much more significant, with a voltage jump after reaching the peak value. The difference between the upward and the downward sweep is more evident at high base accelerations. This type of behavior is consistent with the one observed in other nonlinear energy harvesters, notably in bistable Duffing oscillators (Erturk and Inman, 2011), single-magnet nonlinear piezoelectric converters (Ferrari et al., 2011) and nonlinear electrostatic harvesters (Tvedt et al., 2010).

After decreasing the spacing distance to $\lambda = 0.175$ the response curve shows a even more remarkable stiffening and bending under the same base excitation

(Figure 7). The amplitude voltage at 0.5g is however relatively small compared the analogous one shown in Figure 6, which means that the lower excitation cannot overpower the magnetic force within the system. After overcoming this barrier the unstable region of the system (i.e., the area between the high-energy jump down and the low-energy jump up) becomes however wider. For the case of $\lambda = 0.1375$, the magnetic force provides a bigger effect on the response curve. The system needs now a higher level of excitation to overcome the magnetic field, therefore the system under 1g of excitation still shows an almost linear energy harvesting performance (Figure 8).

Figure 9 shows more specifically the influence of the spacing distance under the same base acceleration of 3g. Figure 9 (a) is related to the response of beams 1 and 3 under the same magnetic force. When the spacing distance is larger and the magnetic force is small, the system can be treated as linear. With the decrease of *d* the unstable region expands and the response curve presents some significant bending. Figure 9 (b) shows the response of beam-2, with the magnetic force acting upon the middle beam being larger than in beams 1 and 3 (see Eq. (15)). The simulations show that the amplitude of beam #2 is slightly larger than the ones of beams #1 and #3, however the unstable regions feature the same degree of variation.

It is evident from these simulations that the E-shape PEH exhibits a significant tunability under different working conditions. Higher magnetic forces can create nonlinear behavior, but also need larger base accelerations. The nonlinear response shows that when the excitation frequency of the system increases towards

high frequencies, the output voltage will follow the upper branch up until the maximum value, followed by a jump down to the low-energy orbit. On the opposite, during the downward sweep the response follows the low-energy orbit at first, and then jumps to the upper branch. These behaviors can also be found in other nonlinear piezoelectric harvesters. In the present work we however combine the concepts of multi-beams vibrational PEHs and the piezomagnetoelastic energy harvester to create a new type of nonlinear system.

5. Experimental results

5.1 Experimental setup and procedures

An E-shape PEH has been fabricated following the guidelines of paragraph 2 to validate the model proposed so far. Within the manufactured prototype the distance between magnets can be changed through the introduction of a slide rail. The three cantilever beams with PZT layers have dimensions $11mm \times 80mm \times 0.7mm$. Based on the results from the simulations, the distance between the two selected magnets are 25mm, 17mm, 14mm and 11mm. When d=25mm the magnetic force assumes a linear behavior and the system therefore can be considered as a linear PEH. The experimental setup is shown in Figure 10. We use a signal generator (80 MHz waveform generator, Agilent 33250A), a power amplifier (LA-200, YMC piezotronics Inc.), a shaker (MS-200, 200N, YMC piezotronics Inc.) and an electrical circuit and oscilloscope (Agilent DSO6034A) with the E-shape EH. The energy harvester is mounted on a shaker that provides the base excitation, with the signal controlled by the signal generator and the power amplifier. The output voltage of the energy

harvester is measured by the oscilloscope.

The piezoelectric layers are connected in parallel, and the polarization orientation of the PZT layers is the same (along the z-direction). The open circuit voltage output of the energy harvester is first trialled, and the nonlinearity behavior of the E-shape energy harvester is compared with the one of the linear system. The forward and backward sweep test is operated within 10Hz to 30Hz at a sweep rate of of 0.1Hz/s. After this experiment, the nonlinear behavior of the E-shape PEH with different magnetic forces is investigated by recording the output voltage in the frequency domain. The frequency bandwidths between the E-shape and the linear energy harvesters are then compared.

5.2 Open-circuit experimental results

In this experiment the energy harvesting performance of the E-shape PEH without magnets is measured in terms of open-circuit output voltage. For this test we have chosen two spacing distances between the three cantilever beams (d=25mm and d=14mm) to investigate the effect of the magnetic force. The open-circuit voltage is measured at 15 Hz and 1.5 g base excitation. Figure 11 shows the voltage response for the case of the linear energy harvesting system (d=25mm) and the nonlinear system. The voltage generated by the E-shape energy harvester at d=14mm shows an obvious nonlinear behavior (blue curve), with a RMS voltage of 4.2 V for d=14mm. The nonlinear behavior of the E-shape energy harvester generates 297% RMS voltage more than the one provided by the linear piezoelectric cantilever beams. The increase of the voltage output from the piezoelectric patches is mainly due to the nonlinear

magnetic force.

5.3 Results related to the energy harvesting experiments

5.3.1 Linear analysis

Figure 9 shows the results from the simulations. The linear case here corresponds to the E-shape PEH with the larger spacing distance (d=25mm), which implies that the effect of the magnetic force is close to zero at that particular spacing distance. The magnetic force in Eq. (15) can be therefore reduced, and the system model is now represented by three linear cantilever beams. The numerical values of the first natural frequency is 24.9Hz. From the experimental results shown in Figure 12 one can observe that the voltage responses of the system are typical of linear PEHs.

The maximum output voltage occurred at 24Hz, 23.9Hz and 24Hz respectively. These values are very close to the numerical first natural frequency. The half-power bandwidth of the linear system is 0.8Hz, and the banwidth for a voltage larger than 10V is 3.7Hz at 0.5g excitation.

5.3.2 The effects of the spacing distance on the harvester performance

For the nolinear case, the voltage-frequency curves tend to veer either towards the left or the right, indicating the presence of a hardening or softening nonlinearity. The veering of the voltage/frequency curves allows to widen the response bandwidth of energy harvesters (Daqaq et al., 2014). It is worth noticing that in the voltage experimental data shown in figures 12 to 15 noise is present when the

frequency is far away from the resonance; this could induce residual output voltage. From the simulations shown in Figure 6 (d=17mm) it is possible to observe that the frequency response curve follows a slight bend when the excitation is at 0.5g. When the excitation level increases the curve tends to bend even more. The frequency domain response with upward and backward sweep at constant excitation acceleration is shown in Figure 13. The dots shown in Figures 13, 14 and 15 are related to the experimental data, while the lines correspond to a fitting using a order three polynomial function.

The maximum output voltage of the E-shape energy harvester at d=17mm is increased with the excitation acceleration (analogous to Figure 6). For a low-level excitation (0.5g) the peak of the response curve is now slightly shifted to 21.3Hz, which implies that the system has a reduced linear stiffness (Tang and Yang, 2012). Furthermore, for the same excitation acceleration the simulation results (Figure 6) show that the peak of the response curve is slightly moved to a frequency of 21.2Hz (the experimental one is 21.3Hz). The upward and downward sweeps do not show remarkable differences. With the increase of the excitation the peaks of the simulated responses are moved to frequencies of 21.6Hz at 1g, 22.1Hz at 2g and 23.2Hz at 3g. We can also observe the change of the peaks in the experiments (Figure 13); in that case the response shows a bend corresponding to 22Hz at 1g, 22.3Hz at 2g and 22.7Hz at 3g. The increase of the excitation has a clear influence on the peak amplitude of the response. For example (beam #1 at 3g excitation), when the frequency increases towards higher values the output voltage grows continuously

from 4.4V at 10Hz to 59.4V at 22.7Hz. After that the voltage jumps down to 6.3V, which indicates that the beam vibrates only around one stable point. When the sweep direction is reversed the voltage increases slowly from 2.9V at 30Hz to 9.4V at 21.4Hz. After that, the output voltage jumps to 45V at 21.3Hz, and then decreases gradually.

For the comparisons between simulations and experiments of the peak voltage when d=17mm, the dimensionless voltage shown in figure 6 should be multiplied by the parameter $V_c = -L\Theta / C_p$, which corresponds to $V_c = 3512$. One can observe that the simulated peak voltages agree well with the experimental ones; for example, when the excitation is equal to 1g, the average experimental peak voltage is 43.7V (41.7V from the simulations, with a 4.6% error). At higher excitations (3g), the peak voltage obtained from the simulations is 70.2V, which is 7% higher than the experimental value.

The spacing distance of the piezoelectric cantilever beam is then reduced to *d*=14mm, which means that the magnetic force of the system becomes larger. The experimental results are shown in Figure 14. The decrease of the spacing distance creates a higher magnetic force, and the system therefore needs more energy to overcome the potential barrier. The bifurcation then occurs at higher base accelerations. For *d*=14mm, a 0.5g excitation can not provide a veer to the right of the voltage-frequency response curve. If the excitation is raised to 1g the frequency response of the energy harvester shows an evident bend, similarly to the simulation results shown in Figure 7. The peak of the response curve is bent at a frequency of

21.1Hz, while the analogous simulation peak is at 21.8Hz). For higher excitations the peaks are bent at 22.2Hz and 23.6 Hz for 2g and 3g, respectively. With the increase of the excitation the frequency response curve tends to bend in a more remarkable way. We can also obseve this variation in the simulations, with the response curve bending at 22.6Hz and 24.2Hz for 2g and 3g, respectively. The computed value of the peak voltage at 1g of excitation is 41.1V (Figure 7), with a 0.5% error against the experimental results shown in Figure14 (41.3V). When the excitation is increased to 3g, the simulated peak voltage (79.8V) is 9.8% larger than the experimental one.

The experimental results shown in Figure 15 are related to a spacing distance further reduced to 11mm. For this bistable configuration, when the excitation acceleration is very small the vibration can not supply sufficient energy for the system to overcome the two potential wells. Similarly to what observed in Figure 8, the 1g excitation cannot create a bend of the frequency response curve. The three beams will therefore vibrate only around one stable point with small amplitudes (small limit cycle oscillations). The system now needs more vibrational energy to cross the potential barriers (almost 2g in terms of excitation, analogous to what present in Figure 8), and the minimum output voltage at 3g of excitation is above 5V. The response curve reaches a peak at 21.5Hz with 2g of excitation, and this value increases to 22.7Hz and 23.6Hz for 3g and 4g, respectively. The simulated peak of the response curve occurs at 21.3Hz for a 2g excitation, and this differs from the experimental case. At 3g and 4g excitations the simulated peaks are bent in the vicinity of 23.3Hz and 25.1Hz. The simulated peak voltage at 1g of excitation shown in Figure 8 is 24.2V, which is higher

than the experimental one (20.3V). When the bease excitation is 2g, the peak voltage obtained from the simulation is now 65.9V, which is 9.7% smaller than the experimental value. The simulation results do however agree well with the experimental ones when the base excitation increases to 4g at d=11mm, with a 0.9% error.

In summary, the comparison between the simulation and the experimental results shows the effect of the magnetic force when the spacing distance d (or the nondimensional parameter λ in the simulations) is decreased. In that case, both the model and the experiments show a frequency-response with a hardening spring behavior that bends the peak towards higher frequencies, and for higher excitation levels this bending becomes more significant. The decrease of the spacing distance can enhance the contribution provided by the magnets, while at the same time the system needs higher excitation levels to overcome the potential barriers. The comparison between the simulation and the experimental results shows in general a quite good agreement of the frequency response behavior.

5.3.3 Bandwidth comparison

The comparison of the bandwidth of the E-shape PEH with different spacing distances is shown in Table 2. The table represents the average half-power bandwidth ($U_{max}/\sqrt{2}$) of the three beams and the frequency range at several specific voltages (10V, 15V and 20V). For the bandwidth comparison, we use in this work the values of the absolute voltages in a similar way to the analysis shown in (Daqaq et al, 2014; Masana and Daqaq, 2011; Pan et al, 2017). The average half-power bandwidth

of the linear energy harvester (d=25mm) is 0.8Hz, which is relatively narrow; the simulated average half-power bandwidth at d=25mm is 0.72Hz, which shows a 10% error. At d=17mm, the simulated half-power bandwidth (1.72 Hz) is now 2.9% higher than the experimental one. As the distance d is decreased to 14mm, both the simulated and experimental half-power bandwidth values are increased (2.13Hz for the simulation and 2.15Hz for the experiment, with a 0.9% error). When the spacing distance is decreased the effect of the magnetic force becomes obvious, and the half-power bandwidth can be expanded to 2.67 Hz at d=11mm (the simulation provides 2.59Hz, which is 3% smaller than the experiment). This bandwidth expansion is significant, leading to a 234% improvement. Moreover, for the same spacing distance the frequency range increases with the base excitations. For output voltages larger than 10V the average bandwidth is 6.9 Hz (d=25mm, 3g excitation). However, when the spacing distance is decreased, the average frequency bandwidth at 10V is significantly improved. When d=11mm the bandwidth improves to 10.4Hz with the same excitation acceleration (3g). The nonlinearity of the system is created by the magnetic force, which is significantly affected by the spacing distance. A bistable nonlinear energy harvester can be obtained by decreasing the spacing distance of the magnets. At low levels of excitation the oscillations of the bistable harvester is confined around one potential well. On the contrary, at higher levels of excitation chaotic oscillations and larger orbit oscillations happen, and the magnitude of the output voltage is significantly improved. The analysis of the frequency bandwidth shows that the decrease of the spacing distance expands the bandwidth of the system.

However, for smaller spacing distances with larger nonlinear forces the harvester will need higher excitation levels to overcome the potential barrier. Appropriate large spacing distances are therefore suitable for low-level excitation environments, but if the excitation is large enough the E-shape energy harvester with small spacing distances could also work effectively.

6. Conclusions

In this work, a novel nonlinear piezoelectric generator for energy harvesting from environmental vibrations has been designed and evaluated. The nonlinear behavior can be obtained by three groups of magnets attached to the free end of the structure. The model of the E-shape energy harvesting system is developed using the Hamilton principle, and the influence of the magnetic force is taken into account. The magnetic force exerted on the system changes by controlling the spacing distance between the three cantilever beams.. The simulations show that the use of a higher magnetic force can create a nonlinear behavior but it also needs larger excitation, and the frequency-response curve will tend to veer towards the right, with jump phenomena during different directions of the frequency sweep. The E-shape PEH has been also evaluated experimentally with different spacing distances at several base excitation accelerations. For the linear case with larger spacing distances the maximum output voltage occurs near the resonant frequency of each beam. When the spacing distance decreases the voltage-frequency curve will bend towards the right and the linear stiffness is reduced. A typical nonlinearity can be observed from both the simulations and the experimental results. The output voltage of the system in the frequency domain shows a general excellent performance, and the frequency bandwidth of the harvested system significantly improves. The average half-power bandwidth of the linear energy harvester at the highest distance is only 0.8Hz. When the spacing between beams is decreased, the effect of the magnetic force becomes more obvious, and the average half-power bandwidth can be expanded up to 2.67 Hz,

which implies that the half-power bandwidth is increased by 2.34 times. Moreover, the frequency range at specific voltage values is larger than the linear case. Compared to conventional cantilever PEHs with traditional tip mass, the energy harvester designed and tested in this work appears to be more suitable for a wide spectrum of environmental vibrational configurations.

Acknowledgement

This work is supported by the National Natural Science Foundation of China (Grant No 11225211) and China Scholarship Council.

References

Abdelkefi A and Barsallo N (2016) Nonlinear analysis and power improvement of broadband low-frequency piezomagnetoelastic energy harvesters. *Nonlinear Dynamics* 83(1-2): 41-56.

Anton S R and Sodano H A (2007) A review of power harvesting using piezoelectric materials (2003–2006). *Smart Materials and Structures* 16(3): R1-R21.

Arnold D P (2007) Review of microscale magnetic power generation. *IEEE Transactions on Megentics* 43(11): 3940-3951.

Arrieta A F, Delpero T, Bergamini A E, et al. (2013) Broadband vibration energy harvesting based on cantilevered piezoelectric bi-stable composites. *Applied Physics Letters* 102(17): 173904.

Betts D, Kim H A, Bowen C R, et al. (2012) Static and Dynamic Analysis of Bistable Piezoelectric Composite Plates for Energy Harvesting. In: *20th ASC structures, structural dynamics and materials conference* AIAA 2012-1492.

Daqaq M F, Masana R, Erturk A, et al. (2014) On the Role of Nonlinearities in Vibratory Energy Harvesting: A Critical Review and Discussion. *Applied Mechanics Reviews* 66(4): 040801.

Erturk A, Hoffman J and Inman D J (2009) A piezomagnetoelastic structure for broadband vibration energy harvesting. *Applied Physics Letters* 94(25): 254102.

Erturk A and Inman D J (2008) On Mechanical Modeling of Cantilevered Piezoelectric Vibration Energy Harvesters. *Journal of Intelligent Material Systems and Structures* 19(11): 1311-1325.

Erturk A and Inman D J (2011) Broadband piezoelectric power generation on high-energy orbits of the bistable Duffing oscillator with electromechanical coupling. *Journal of Sound and Vibration* 330(10): 2339-2353.

Ferrari M, Bau M, Guizzetti M, et al. (2011) A single-magnet nonlinear piezoelectric converter for enhanced energy harvesting from random vibrations. *Sensors and Actuators A: Physical* 172(1): 287-292.

Ferrari M, Ferrari V, Guizzetti M, et al. (2010) Improved energy harvesting from wideband vibrations by nonlinear piezoelectric converters. *Sensors and Actuators A: Physical* 162(2): 425-431.

Harne R L, Thota M and Wang K W (2013) Bistable energy harvesting enhancement with an auxiliary linear oscillator. *Smart Materials & Structures* 22(12): 125028.

Harne R L and Wang K W (2013) A review of the recent research on vibration energy harvesting via bistable systems. *Smart Materials & Structures* 22(2): 023001.

Kim H S, Kim J H and Kim J (2011) A Review of Piezoelectric Energy Harvesting Based on Vibration. *International Journal of Precision Engineering and Manufacturing* 12(6): 1129-1141.

Kim M, Hoegen M, Dugundji J et al. (2010) Modeling and experimental verification of proof mass effects on vibration energy harvester performance. *Smart Materials and Structures* 19(4): 069801.

Kim P and Seok J (2014) A multi-stable energy harvester: Dynamic modeling and bifurcation analysis. *Journal of Sound and Vibration* 333(21): 5525-5547.

Laura P A A, Pombo J L and Susemihl E A (1974) A note on the vibrations of a

clamped-free beam with a mass at the free end. *Journal of Sound and Vibration* 37(2): 161-168.

Lu Q, Liu L, Lan X, et al. (2016) Dynamic responses of SMA-epoxy composites and application for piezoelectric energy harvesting. *Composite Structures* 153: 843-850.

Mann B P and Sims N D (2009) Energy harvesting from the nonlinear oscillations of magnetic levitation. *Journal of Sound and Vibration* 319(1-2): 515-53.

Masana R and Daqaq M F (2011) Electromechanical Modeling and Nonlinear Analysis of Axially Loaded Energy Harvesters. *Journal of Vibration and Acoustics* 133(1): 011007.

Mitcheson P, Miao P, Start B, et al. (2004) MEMS electrostatic micropower generator for low frequency operation. *Sensors and Actuators A: Physical* 115(2-3): 523-529.

Pan D, Ma B and Dai F (2017) Experimental investigation of broadband energy harvesting of a bi-stable composite piezoelectric plate. *Smart Materials and Structures* 26(3): 035045.

Paknejad A, Rahimi G, Farrokhabadi A, et al. (2016) Analytical solution of piezoelectric energy harvester patch for various thin multilayer composite beams. *Composite Structures* 154: 694-706.

Priya S (2007) Advances in energy harvesting using low profile piezoelectric transducers. *Journal of Electroceramics* 19(1):167-184.

Qi S, Shuttleworth R, Oyadiji S O, et al. (2010) Design of a multiresonant beam for broadband piezoelectric energy harvesting. *Smart Materials and Structures* 19(9): 094009.

Rafique S and Bonello P (2010) Experimental validation of a distributed parameter piezoelectric bimorph cantilever energy harvester. *Smart Materials and Structures* 19(9): 094088.

Ramezanpour R, Nahvi H and Ziaei-Rad S (2016) A vibration-based energy harvester suitable for low-frequency, high-amplitude environments: Theoretical and experimental investigations. *Smart Materials and Structures* 27(5): 642-665.

Ramlan R, Brennan M J and Mace B R (2009) Potential benefits of a non-linear stiffness in an energy harvesting device. *Nonlinear Dynamics* 59(4): 545-558.

Ren L, Liu Y M, Geng X, et al. (2006) Single Crystal PMN-PT /Epoxy 1-3 Composite for Energy Harvesting Application. *IEEE Transactions on Ultrasonics Ferroelectrics and Frequency Control* 53(3): 631-637.

Roundy S and KWright P (2004) A piezoelectric vibration based generator for wireless electronics. *Smart Materials and Structures* 13(5): 1131-1142.

Shahruz S M (2006) Design of mechanical band-pass filters with large frequency bands for energy scavenging. *Mechatronics* 16(9): 523-531.

Sodano H A, Inman D J and Park G (2005) Comparison of piezoelectric energy harvesting devices for recharging batteries. *Journal of Intelligent Material Systems and Structures* 16(10): 799-807.

Song H J, Choi Y T, Wereley N M, et al. (2010) Energy Harvesting Devices Using Macro-fiber Composite Materials. *Journal of Intelligent Material Systems and Structures* 21(6): 647-658.

Stanton S C, McGehee C C and Mann B P (2010) Nonlinear dynamics for broadband

energy harvesting: Investigation of a bistable piezoelectric inertial generator. *Physica: D Nonlinear Phenomena* 239(10): 640-653.

Su W J, Zu J and Zhu Y (2014) Design and development of a broadband magnet-induced dual-cantilever piezoelectric energy harvester. *Journal of Intelligent Material Systems and Structures* 25(4): 430-442.

Tang L and Yang Y (2012) A nonlinear piezoelectric energy harvester with magnetic oscillator. *Applied Physics Letters* 101(9): 094102.

Tang L, Yang Y and Soh C K (2012) Improving functionality of vibration energy harvesters using magnets. *Journal of Intelligent Material Systems and Structures* 23(13): 1433-1449.

Tvedt L G W, Nguyen D S and Halvorsen E (2010) Nonlinear Behavior of an Electrostatic Energy Harvester under Wide- and Narrowband Excitation. *Journal of Microelectromechanical System* **19**(2): 305-316.

Twiefel J and Westermann H (2013) Survey on broadband techniques for vibration energy harvesting. *Journal of Intelligent Material Systems and Structures* 24(11): 1291-1302.

Westermann H, Neubauer M and Wallaschek J (2012) Modeling of A Vibration-based Piezomagnetoelastic Energy Harvesting System by Using the Duffing Equation. *Proceedings of the ASME Conference on Smart Materials, Adaptive Structures and Intelligent Systems* 2: 803-810.

Williams C B and Yates R B (1996) Analysis of a micro-electric generator for microsystems. *Sensors and Actuators A: Physical* 52(1-3): 8-11.

Wu Z, Harne R L and Wang K W (2014) Energy harvester synthesis via coupled linear-bistable system with multistable dynamics. *Journal of Applied Mechanics* 81(6): 061005.

Xu T B, Siochi E J, Kang J H, et al. (2013) Energy harvesting using a PZT ceramic multilayer stack. *Smart Materials and Structures* 22(6): 065015.

Xue H, Hu Y T and Wang Q M (2008) Broadband piezoelectric energy harvesting devices using multiple bimorphs with different operating frequencies. *IEEE Transactions on Ultrasonics Ferroelectrics and Frequency Control* 55(9): 2104-2108.

Zhou S, Cao J, Inman D J, et al. (2014) Broadband tristable energy harvester: Modeling and experiment verification. *Applied Energy* 133: 33-39.

Figure Captions

Figure 1. Schematic view of the magnet-induced bistable piezoelectric energy harvesting system.

Figure 2. Magnetic force model in the E-shape system

Figure 3. Simulated results for the magnetic force along the z-axis at different spacing distances

Figure 4. Magnets configuration for the energy harvester

Figure 5. Experimental FRF curve of the cantilever beam

Figure 6. The voltage response at different excitation accelerations with $\lambda = 0.2125$

Figure 7. The voltage response at different excitation accelerations with $\lambda = 0.175$

Figure 8. The voltage response at different excitation accelerations for $\lambda = 0.1375$

Figure 9. The voltage response at different spacing distance with 3g excitation (a) Beam-1, 3; (b) Beam-2

Figure 10. Schematic of the experimental setup

Figure 11. Open-circuit voltage of the system without electrical load at 15Hz

Figure 12. The voltage-frequency curves for d=25mm, and base acceleration of 0.5 g (Left) and 1 g (Right)

Figure 13. Voltage-frequency curves with different excitation accelerations for a spacing distance of *d*=17mm (From left to right are beam-1, beam-2, beam-3)

Figure 14. Frequency-response curves of the output voltage amplitude with different excitation accelerations for a spacing distance *d*=14mm (From left to right are beam-1, beam-2, beam-3)

Figure 15. Frequency-response curves of the output voltage amplitude with different excitation acceleration when spacing distance *d*=11mm (From left to right are beam-1, beam-2, beam-3)

Table Captions

Table 1. Basic material property

Table 2. Bandwidth comparison with different spacing distances

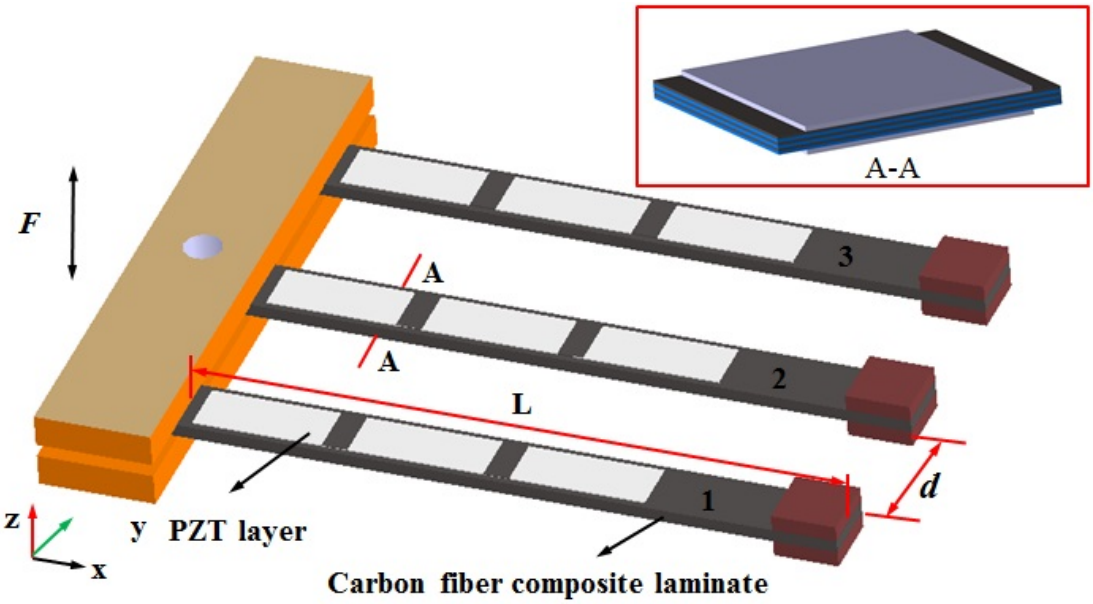

Figure 1. Schematic view of the magnet-induced bistable piezoelectric energy harvesting system.

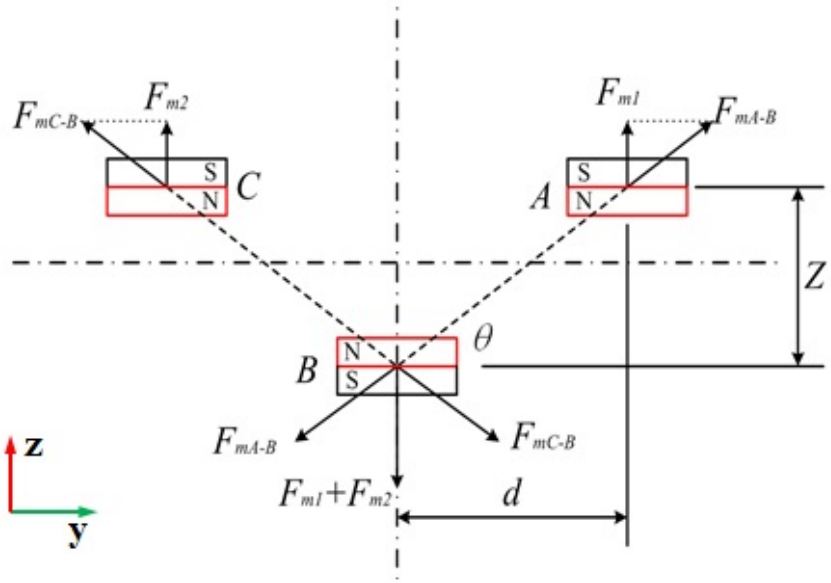

Figure 2. Magnetic force model in the E-shape system

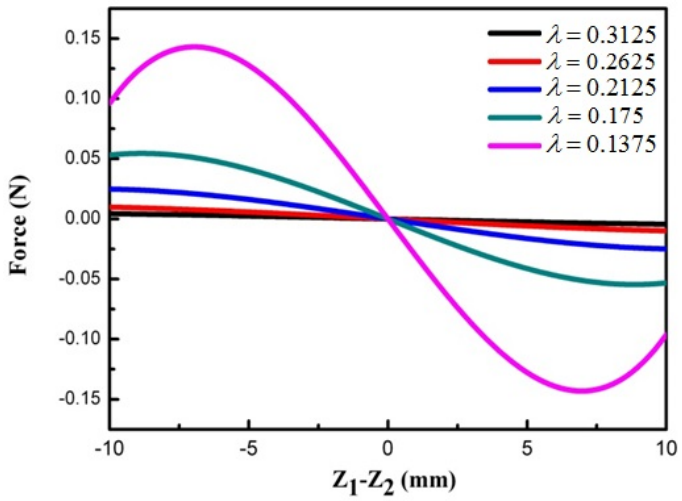

Figure 3. Simulated results for the magnetic force along the z-axis at different spacing distances

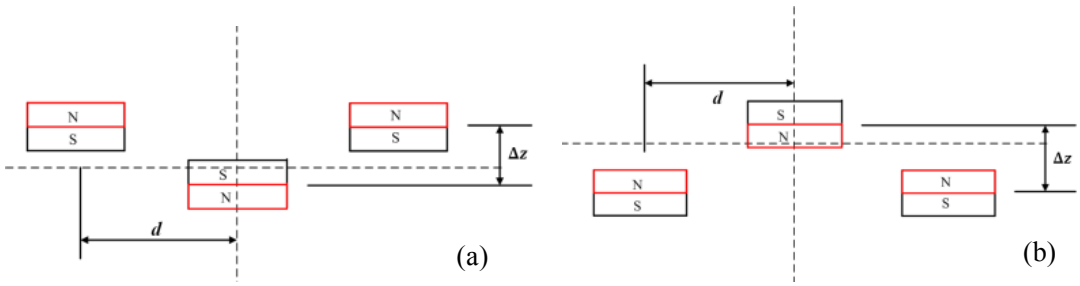

(a) Stable state 1, (b) Stable state 2

Figure 4. Magnets configuration for the energy harvester

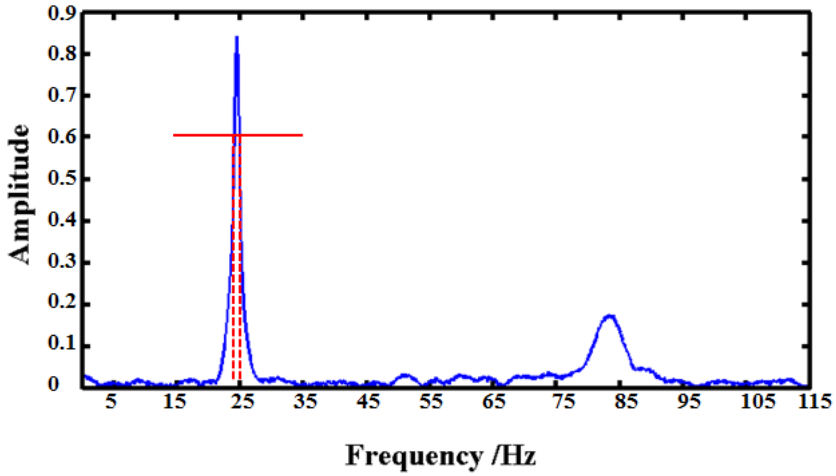

Figure 5. Experimental FRF curve of the cantilever beam

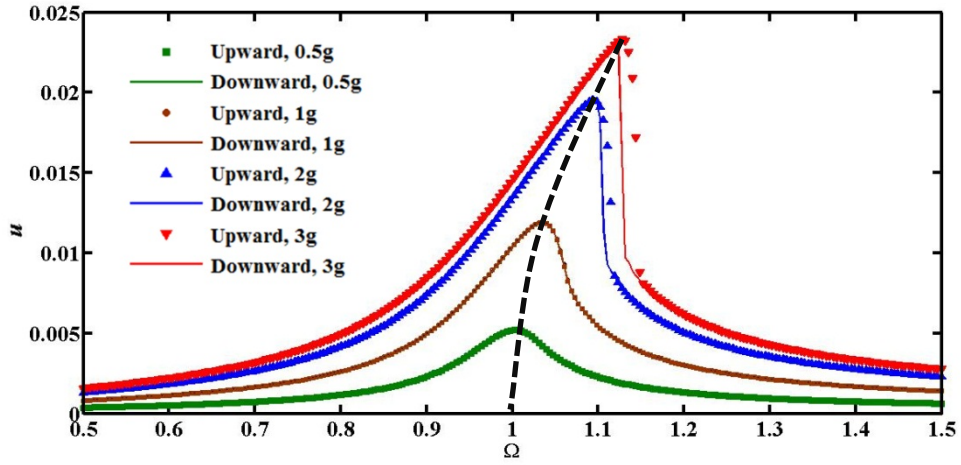

Figure 6. The voltage response at different excitation accelerations with $\lambda = 0.2125$

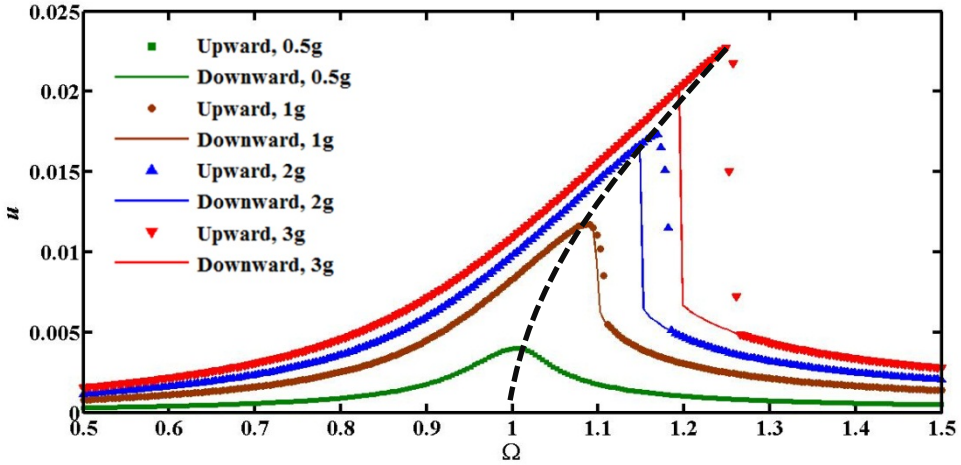

Figure 7. The voltage response at different excitation accelerations with $\lambda = 0.175$

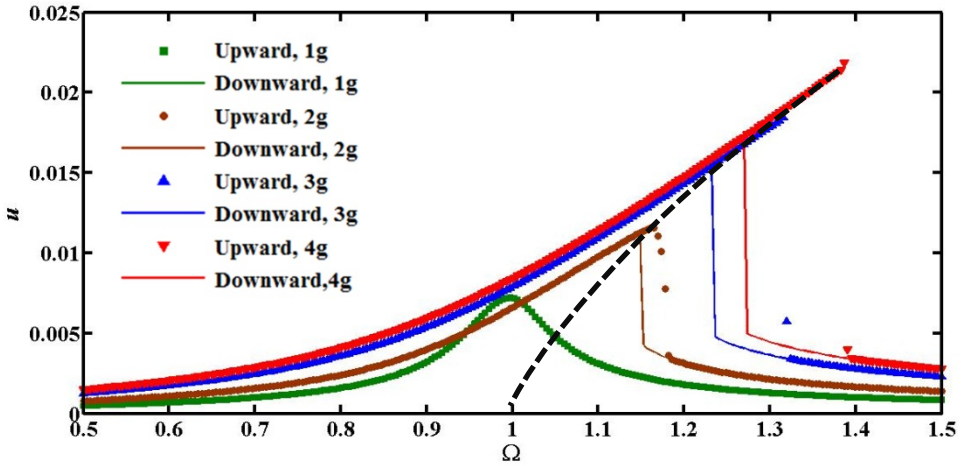

Figure 8. The voltage response at different excitation accelerations for $\lambda = 0.1375$

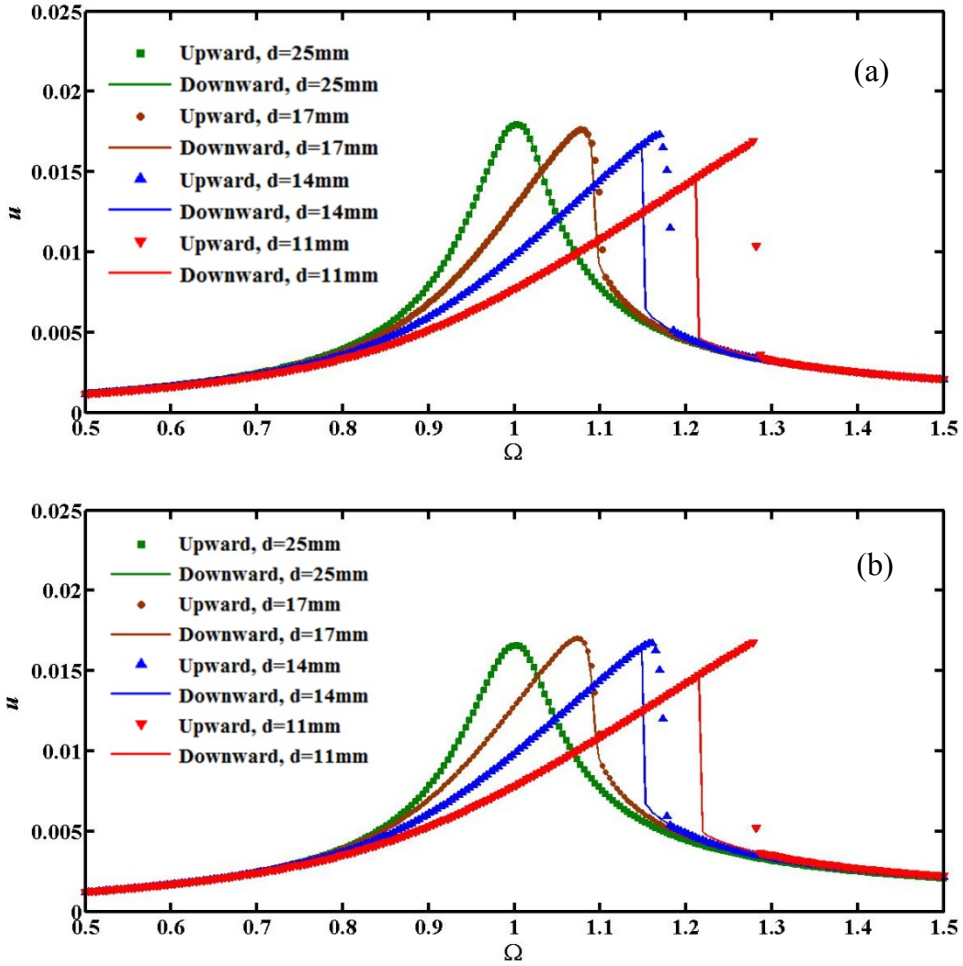

Figure 9. The voltage response at different spacing distance with 3g excitation (a) Beam-1, 3; (b) Beam-2

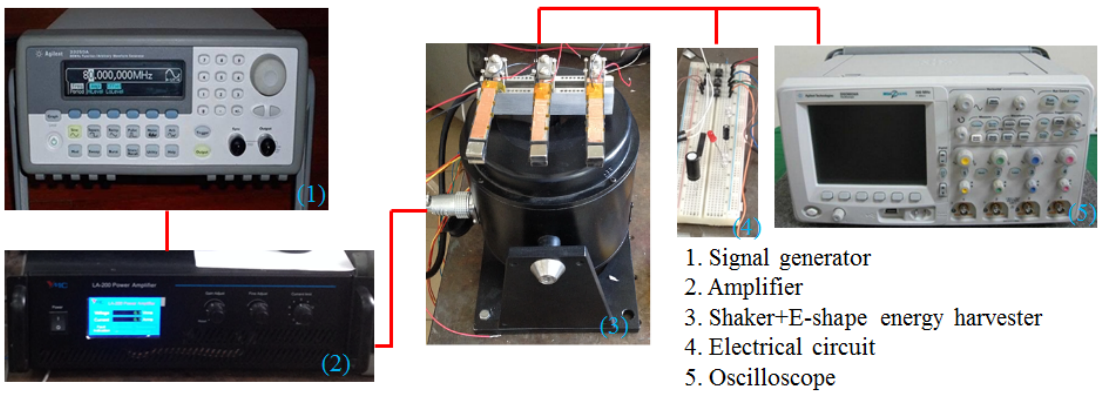

Figure 10. Schematic of the experimental setup

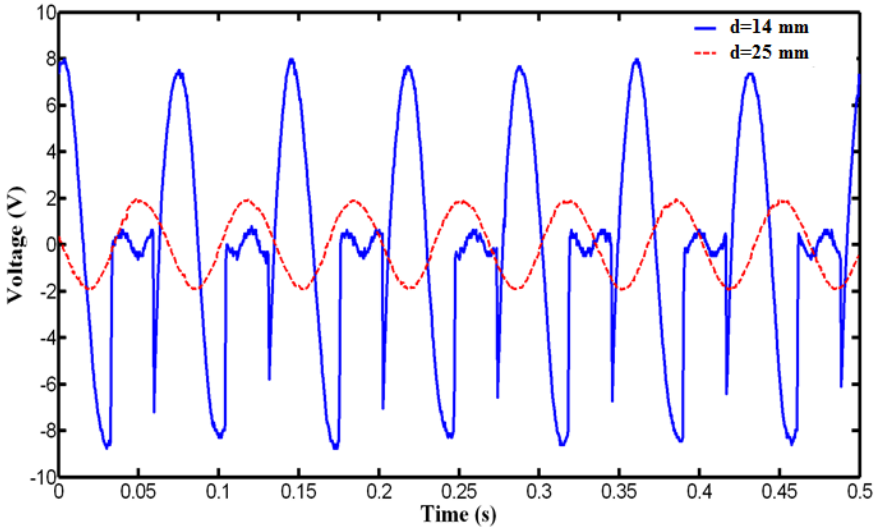

Figure 11. Open-circuit voltage of the system without electrical load at 15Hz

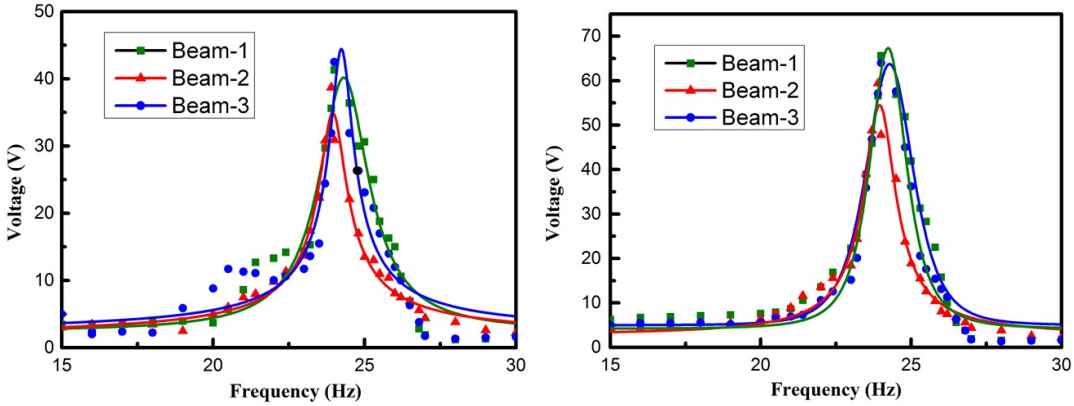

Figure 12. The voltage-frequency curves for d=25mm, and base acceleration of 0.5 g (Left) and 1 g (Right)

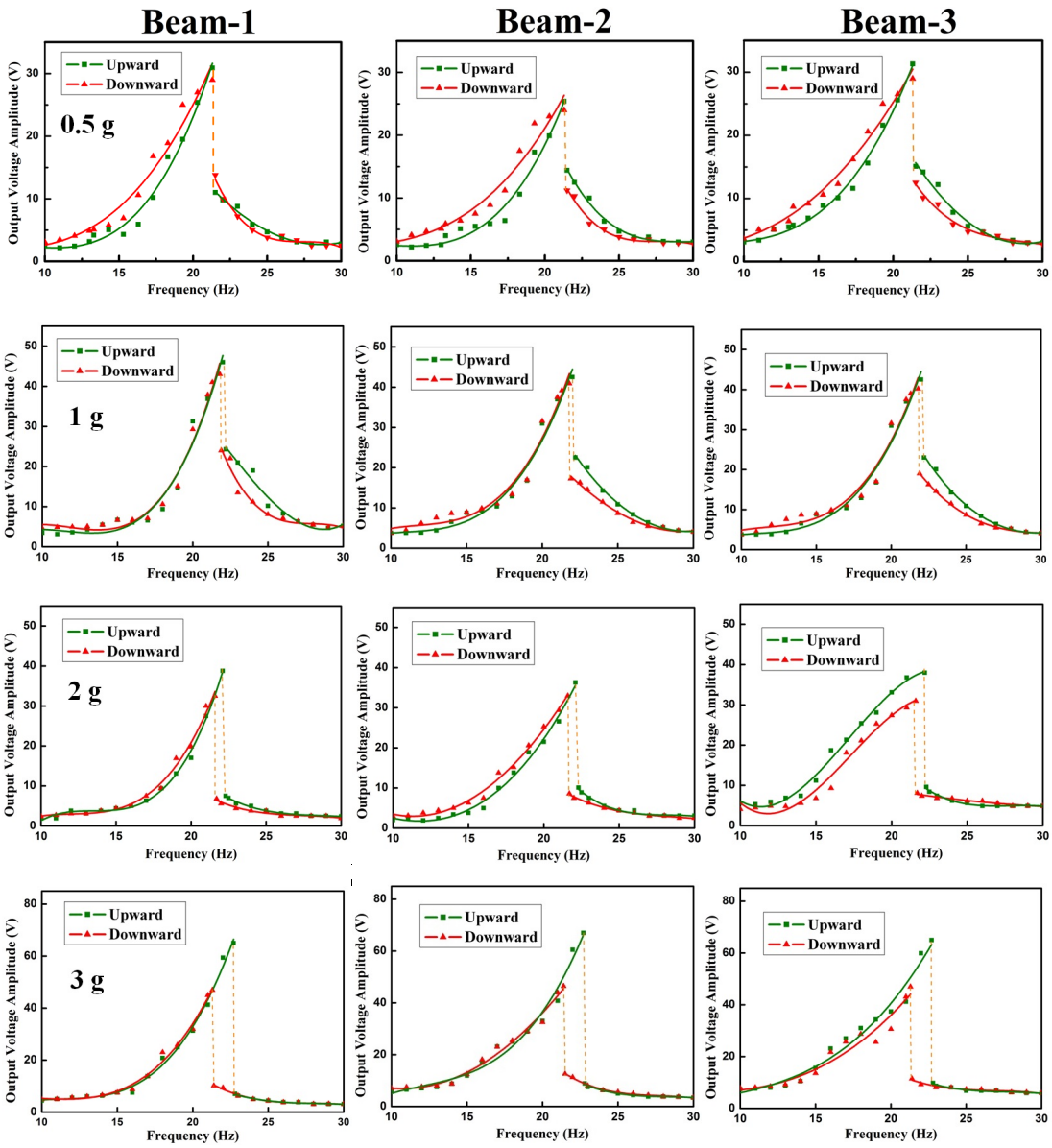

Figure 13. Voltage-frequency curves with different excitation accelerations for a spacing distance of *d*=17mm (From left to right are beam-1, beam-2, beam-3)

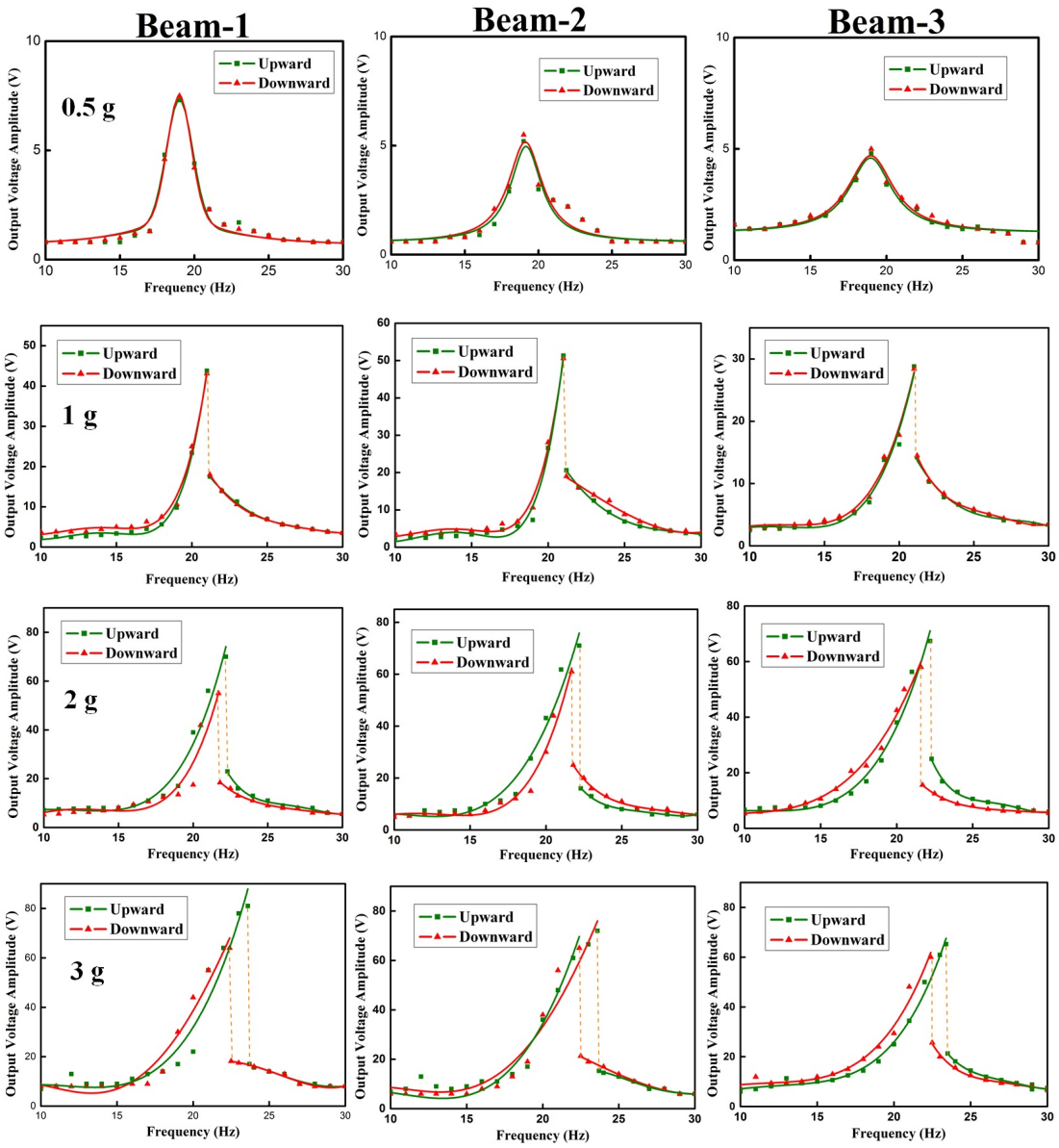

Figure 14. Frequency-response curves of the output voltage amplitude with different excitation accelerations for a spacing distance *d*=14mm (From left to right are beam-1, beam-2, beam-3)

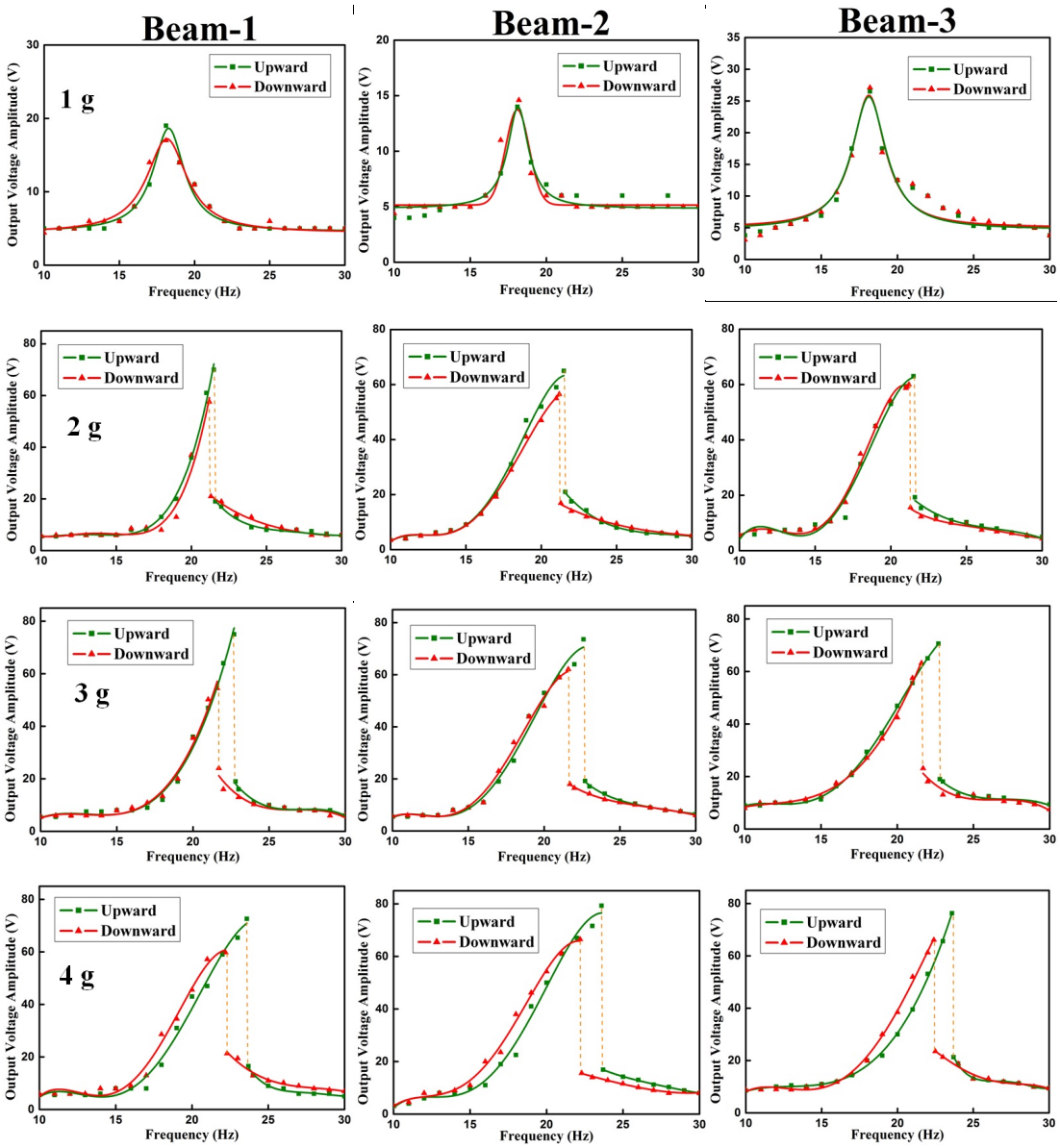

Figure 15. Frequency-response curves of the output voltage amplitude with different excitation acceleration when spacing distance *d*=11mm (From left to right are beam-1, beam-2, beam-3)

Table 1. Basic material property

Properties	CFRP	PZT-5H	Magnet
Density/(kg/m^3)	1600	7800	7500
Length/(mm)	80	60	10
Width/(mm)	11	10	10
Thickness/(mm)	0.7	0.2	2.5
Modulus/(GPa)	$E_1 = 125GPa$ $E_2 = 9GPa$ $G_{12} = 3.7GPa$	60.6	150
Poisson's ratio	0.33	0.289	--
Piezoelectric stress constants/(C/m^2)	--	-17.15	--
Absolute permittivity/(F/m)	--	3800	--
Moments of magnetic dipoles/(Am^2)	--	--	0.019

Table 2. Bandwidth comparison with different spacing distances

Spacing distance	Half-power bandwidth		Excitation acceleration	Frequency bandwidth (≥10V)	Frequency bandwidth (≥15V)	Frequency bandwidth (≥20V)
	Simulation	Experiment				
d=25mm	0.72Hz	0.8 Hz	0.5g	3.7 Hz	2.4 Hz	1.6 Hz
			1g	5 Hz	3.6 Hz	3.1 Hz
			2g	6.1 Hz	4.7 Hz	3.8 Hz
			3g	6.9 Hz	5.4 Hz	4.4 Hz
d=17mm	1.72Hz	1.67 Hz	0.5g	4.4 Hz	2.7 Hz	1.8 Hz
			1g	6.8 Hz	5.4 Hz	3.7 Hz
			2g	6.5 Hz	5.6 Hz	4.5 Hz
			3g	7.7 Hz	6.7 Hz	5.9 Hz
d=14mm	2.13Hz	2.15 Hz	1g	5.1 Hz	3.1 Hz	1.6 Hz
			2g	8.1 Hz	5.9 Hz	4.6 Hz
			3g	10.2 Hz	6.3 Hz	4.9 Hz
			4g	12.2 Hz	6.7 Hz	5.2 Hz
d=11mm	2.59Hz	2.67 Hz	1g	3.2Hz	2.1Hz	--
			2g	8.8 Hz	6.1 Hz	4.8 Hz
			3g	10.4 Hz	7.1 Hz	5.3 Hz
			4g	16 Hz	8.4 Hz	6.8 Hz

g=9.8 m/s^2